Acta Oceanol. Sin., 2026, Vol. 45, No. 9, P. 1–13
https://doi.org/10.1007/s13131-026-2700-8

A modified thermal lag correction method for glider-based salinity measurements

Xue Sun[1], Hongyang Lin[1, 2, 3*], Zhiyu Liu[1, 2, 3*], Zhendong Hu[1], Jiancheng Yu[3, 4], Minhan Dai[1, 2, 3]

[1] State Key Laboratory of Marine Environmental Science and College of Ocean and Earth Sciences, Xiamen University, Xiamen 361102, China
[2] Laoshan Laboratory Fujian Institute, Xiamen 361102, China
[3] Fujian Ocean Innovation Center, Xiamen 361102, China
[4] Shenyang Institute of Automation, Chinese Academy of Sciences, Shenyang 110169, China

Received 28 December 2025; accepted 27 April 2026
© Chinese Society for Oceanography and Springer-Verlag GmbH Germany, part of Springer Nature 2026

Abstract
This study introduces a new approach, termed the weighted method, for thermal lag correction in glider-based salinity measurements. The method implements an isopycnal-dependent weighting scheme to combine two salinity datasets: (1) data corrected using the Garau method (using downcast and upcast from a single dive as reference profiles) and (2) data corrected using the anti-Garau method (using downcast from a dive and upcast from its preceding dive as reference profiles). Operating in isopycnal coordinates, the weighted method naturally removes distortions caused by internal wave-induced isopycnal displacements. Comparative analysis demonstrates the weighted method's superior performance over existing approaches. A key advantage of the weighted method is that it does not rely on predefined division points, thus avoiding artificial salinity spikes as seen in the segmented method, and maintains profile smoothness throughout the water column. Also, salinity profiles corrected by the weighted method show promising agreement with the synchronous SBE 911plus CTD measurements, confirming the feasibility of using this method to obtain reliable glider-measured salinity data. Notably, the method may not work well in frontal zones because the glider's downcast and upcast could actually sample distinct water masses which does not satisfy the presumption for thermal lag correction.

Key words thermal lag correction, glider-based salinity measurement, weighted method, isopycnal coordinates

Citation Sun Xue, Lin Hongyang, Liu Zhiyu, Hu Zhendong, Yu Jiancheng, Dai Minhan. 2026. A modified thermal lag correction method for glider-based salinity measurements. Acta Oceanologica Sinica, 45(9): 1–13, doi: 10.1007/s13131-026-2700-8

1 Introduction

Underwater gliders (hereafter referred to as gliders), a specialized category of autonomous underwater vehicles, were first conceptualized by Henry Stommel in the late 1980s (Stommel, 1989). These innovative platforms are specifically engineered for oceanography observations, utilizing a network of small, cost-effective units. Gliders achieve autonomous navigation through buoyancy control for vertical displacement and wing angle adjustments for horizontal propulsion (Rudnick, 2016; Rudnick et al., 2004). This unique integration of vertical and horizontal mobility generates a distinctive sawtooth trajectory, enabling comprehensive three-dimensional sampling of the ocean environment.

Gliders, despite their relatively simple platform design, have been successfully integrated with a variety of advanced sensors, including Conductivity-Temperature-Depth (CTD) sensors. While temperature measurements are obtained directly, salinity is derived from measured temperature and conductivity according to the equation of state of seawater (Fofonoff and Millard, 1983). Consequently, temporal and spatial mismatches between temperature and conductivity measurements can significantly

Foundation item: The National Key Research and Development Program of China under contract Nos 2023YFC3107604 and 2022YFA1003804; the National Natural Science Foundation of China under contract Nos 42076009 and 41730533; the Fundamental and Interdisciplinary Disciplines Breakthrough Plan of the Ministry of Education of China under contract No. JYB2025XDXM801.
*Corresponding author, E-mail: hylin@xmu.edu.cn; zyliu@xmu.edu.cn

compromise the accuracy of salinity estimates (Lueck, 1990; Lueck and Picklo, 1990; Morison et al., 1994). These measurement inconsistencies primarily originate from three fundamental sources: (1) the physical separation between the thermistor and conductivity cell, (2) different response times of the sensors, and (3) thermal lag effects caused by heat storage within the conductivity cell (Johnson et al., 2007; Morison et al., 1994). Among these factors, thermal lag effects exhibit the most pronounced temporal influence, with response times typically on the order of 10 s (Johnson et al., 2007). The thermal lag effect occurs because, as the glider moves through temperature gradients, heat stored in the conductivity cell exchanges with the surrounding water, which alters the conductivity measured inside the cell (Garau et al., 2011). In contrast, the temperature sensor measures the temperature outside the cell. This process creates a temperature discrepancy between the cell interior (where conductivity is measured) and the external environment (where temperature is recorded), introducing errors in derived salinity values. This effect is particularly evident for glider-measured salinity in regions with strong temperature gradients (e.g., thermoclines), and has been widely studied in oceanographic research. For example, Lueck and Picklo (1990) pioneered a numerical model to estimate conductivity at the thermistor location for Sea-Bird conductivity cells. Morison et al. (1994) proposed an approach that minimizes salinity separation of temperature-salinity (*T*-*S*) curves from downcast and upcast of a yo-yo sequence of CTD profiles.

Unlike conventional CTD systems, thermal lag correction for Glider Payload CTD (GPCTD) presents significantly greater challenges due to three key factors: (1) Variable profiling speed. Influenced by buoyancy adjustments, altitude changes, and depth variations (Liu et al., 2015), it is difficult for gliders to maintain a constant profiling speed that could be typically achieved in shipboard CTD. (2) Low sampling frequency. GPCTDs typically sample at 0.5−1.0 Hz, much lower than conventional CTDs (24 Hz). (3) Irregular sampling intervals. Even if programmed with a constant sampling rate, the glider sampling interval often ends up to be irregular (Garau et al., 2011). These operational characteristics render traditional correction techniques inadequate for GPCTD systems.

To address these challenges, Garau et al. (2011) developed a novel methodology specially designed to correct thermal lag errors for unpumped CTD sensors deployed on Slocum gliders, taking into account the variations in glider speed. Subsequent improvements to Garau's method introduced a median filter, enhancing its capability to process salinity measurements in regions with strong thermoclines (Liu et al., 2015). Troupin et al. (2015) later extended Garau's approach to pumped CTD systems and provided MATLAB programs (https://github.com/socib/glider_toolbox). More recent advancements have adopted a segmented approach to thermal lag correction. For instance, Chu et al. (2020) implemented a five-part segmentation of salinity data based on the depth variation and descending speed, while Wang et al. (2020) proposed dividing each downcast and upcast profile into two segments, utilizing temporal and spatial adjacent segments for mutual calibration.

While these studies have established solid foundations for GPCTD thermal lag correction, most existing approaches analyze downcast and upcast profiles in depth or pressure coordinates. Such frameworks failed to account for the vertical undulation of isopycnals caused by, for example, passing internal waves. To this end, we propose an isopycnal coordinate-based correction approach that inherently eliminates distortions caused by internal wave-induced isopycnal displacements. Building on the segmentation concept, we develop a linear weighting scheme (termed the "weighted method"; see Section 3.2.3) for thermal lag correction. This method uses an isopycnal-dependent weighting function by preserving both spatial and temporal consistency across reference profiles.

The structure of this paper is organized as follows: Section 2 introduces the observational data collected by gliders, and procedures for data preprocessing and quality control. Section 3 presents principles for thermal lag correction and introduces three implementation methodologies: the Garau method, the segmented method, and our weighted method. Section 4 compares the performance of the weighted method with existing methods as well as observations made by the shipboard SBE 911plus CTD. Section 5 discusses the impact of the presence of fronts on correcting salinity profiles, and also the limitations of the proposed method. Finally, key findings and conclusions are summarized in Section 6.

2 Data and methods

2.1 *Field observations*

From March 17 to April 17, 2019, a research cruise aboard R/V *Tan Kah Kee* was conducted in the North Pacific Subtropical Countercurrent (STCC) region to investigate physical-biogeochemical interactions within mesoscale eddies (Hu et al., 2023; Fig. 1). During this cruise, a fleet of 11 Sea-Wing gliders, developed by Shenyang Institute of Automation, Chinese Academy of Sciences, was deployed to investigate a cyclonic eddy. These gliders collected high-resolution measurements of temperature, salinity, and various biogeochemical variables (e.g., chlorophyll, dissolved oxygen). Two types of gliders with distinct configurations were deployed: the shallow-diving gliders that are capable of reaching a depth of 300 m with approximately 1 km horizontal spacing between consecutive surface profiles, and the deep-diving gliders operating to 1 000 m deep with 2−3 km horizontal spacing. In this study, we focus on data collected by glider 300K001, a shallow-diving platform operating at a sampling rate of 0.5 Hz. This glider's dataset serves as the primary basis

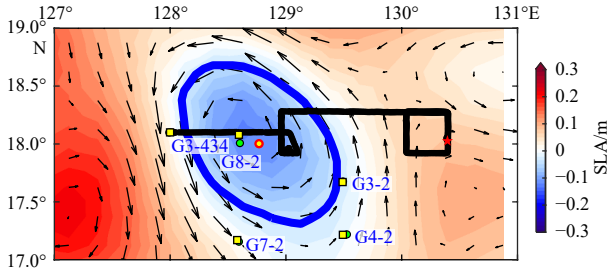


Fig. 1. Observed cyclonic eddy superimposed with the glider trajectory in the study region [the North Pacific Subtropical Countercurrent region (STCC; 17°−19°N, 127°–131°E)]: The figure shows sea level anomalies [SLA, color shading; data obtained from Copernicus Marine Environment Monitoring Service (CMEMS), 0.25° × 0.25° horizontal resolution] overlaid with surface geostrophic currents (black arrows) on April 5, 2019. The blue curve and the red circle mark the edge and center of the observed eddy (identified via py-eddy-tracker; Mason et al., 2014; Pegliasco et al., 2022). The black line traces the trajectory of glider 300K001, and the red pentagram marks its deployment location. The green circles and yellow rectangles represent the sampling locations of selected Glider Payload CTD (GPCTD) and the corresponding SBE 911plus CTD profiles used to validate the salinity correction, respectively. The texts next to the green circles represent the identifier of glider profiles; for example, "G3-2" represents profile pair of G3 glider's second dive measurement.

for demonstrating our data processing methodology and thermal lag correction steps.

2.2 *Satellite data*

The satellite altimeter data are obtained from the Copernicus Marine Environment Monitoring Service (CMEMS, https://marine.copernicus.eu/), including the daily gridded Sea Level Anomaly (SLA), and its associated geostrophic current anomalies at 0.25°×0.25° resolution. The daily SST of Himawari-8 is downloaded from the Japan Aerospace Exploration Agency (https://www.eorc.jaxa.jp/ptree/index.html).

2.3 *Data processing and quality control steps*

The data processing and quality control for GPCTD salinity measurements are comprised of three sequential steps: (1) data preprocessing, (2) sensor correction, and (3) thermal lag correction and final filtering.

2.3.1 *Data preprocessing*

The preprocessing step involves identification and removal of abnormal data according to the following criteria. (1) Profiles containing only downcast or upcast data. (2) Profiles with consistently zero pressure or anomalous pressure readings; In this study, data points with a pressure difference greater than 2 m between adjacent samples are defined as pressure-anomalous data. If such anomalous data points exceed 10 within a single glider dive cycle, the entire profile is classified as a pressure-anomalous profile. If the number of anomalous data points is less than 10, the profile data is retained, but the corresponding values are set to NaN. (3) Profiles with discontinuous sampling times. (4) Profiles exhibiting high-frequency pressure oscillations. (5) Profiles whose maximum sampling depth is significantly shallower than the glider's preset depth.

Among the 499 pairs of profiles collected by glider 300K001, four pairs of abnormal profiles (the 1st, 52nd, 328th and 444th profiles) were identified and excluded from further analysis (Fig. S1). Profile 1 was excluded because its maximum sampling depth of approximately 120 m was significantly shallower than the glider's preset depth. Profiles 52 and 328 were classified as pressure-anomalous profiles, while Profile 444 consisted of no downcast profile.

2.3.2 *Sensor correction*

The sensor correction process eliminates the short-time mismatches between the thermistor and conductivity cell measurements, primarily caused by their physical separation and differing response time. Although previous studies (e.g., Johnson et al., 2007) have shown that errors caused by these short-time mismatches are generally smaller than thermal lag errors, Bishop (2008) suggested that sensor correction effectively reduces small-scale salinity spikes. Our analyses of 495 pairs of salinity profiles from glider 300K001 confirm that sensor correction significantly smooths out small-scale fluctuations in observed salinity profiles (compare black and green profiles in Fig. 2). To solve the short-time mismatching issue, two parameters are adopted during the sensor correction process, namely the time shifts for temperature (τ_t) and conductivity (τ_c). After a systematic test, a pair of suitable time shifts was set to $\tau_t = 0.7$ s and $\tau_c = 0.5$ s.

2.3.3 *Thermal lag correction and final filtering*

The fundamental scientific hypothesis of thermal lag correction is that two mutually corrected reference profiles measure the same water column. Hence, after sensor correction, the thermal lag correction is implemented by minimizing salinity differences between the downcast and upcast reference profiles (detailed in Section 3). Finally, we apply a median filter with a window length of seven data points (Liu et al., 2015) to the thermal-lag-corrected salinity data, producing the final "corrected salinity" profiles.

Using a pair of representative profiles, Fig. 2 illustrates an example showing the progressive improvement in salinity data through each processing step mentioned above. The original downcast and upcast salinity profiles exhibit a significant mismatch (black lines in Fig. 2), especially between potential density σ_θ = 23.5 kg/m^3 and σ_θ = 25.0 kg/m^3 isopycnal surfaces. After sensor correction, a notable reduction in small-scale salinity spikes is

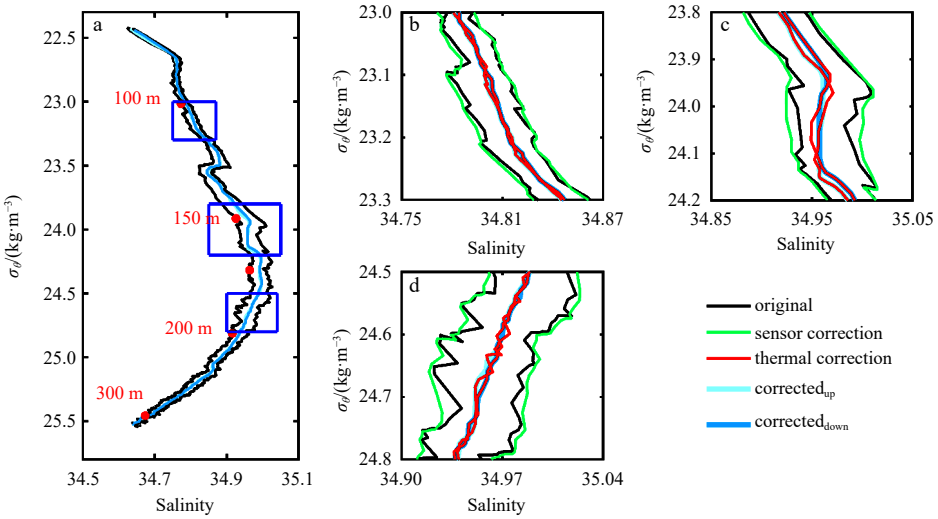


Fig. 2. A correction example using a pair of salinity profiles in isopycnal coordinates (σ_θ denotes potential density). a. The original and corrected entire downcast and upcast salinity profiles and b–d. the enlarged views of the progressive improvement in salinity data highlighted by blue boxes in a. The red dots in a mark the depths of 100 m, 150 m, 200 m, and 300 m. The black lines represent the original salinity calculated from measured temperature and conductivity, the green lines represent the salinity after sensor correction, the red lines represent the salinity after thermal lag correction, while the thick light and dark blue lines indicate the corrected salinity for the upcast (corrected$_{up}$) and downcast (corrected$_{down}$) profiles with a median filter, respectively. The salinity after each correction step is plotted in its respective isopycnal coordinate (i.e., raw salinity on the original isopycnal coordinates, sensor corrected salinity on the sensor corrected isopycnal coordinates, thermal lag corrected salinity on the thermal lag corrected isopycnal coordinates, and so on).

observed (green lines in Fig. 2), and the thermal lag correction dramatically reduces salinity differences between downcast and upcast profiles (red lines in Fig. 2). A subsequent median filter further smooths out small-scale fluctuations in the thermal lag corrected salinity profiles (light and dark blue lines in Fig. 2) while preserving essential oceanographic features. The final corrected profiles exhibit a much better agreement between the downcast and upcast measurements, demonstrating that the thermal lag errors have been eliminated, and that the corrected salinity data can be used for subsequent scientific analysis and interpretation.

2.4 *Statistical quantities for evaluations*

To conduct quantitative comparisons of the three methods in correcting salinity profiles, we use a set of statistical quantities as follows.

(1) Salinity difference (SD) and absolute mean salinity difference (AMSD)

$$\mathrm{SD} = S_\mathrm{d} - S_\mathrm{u}, \tag{1}$$

$$\mathrm{AMSD} = \sum_{i=1}^{N} \frac{1}{N} |\mathrm{SD}_i|, \tag{2}$$

$$\mathrm{AMSD}_{\text{ver-avg}} = \sum_{j=1}^{M} \frac{1}{M} \sum_{i=1}^{N} \frac{1}{N} |\mathrm{SD}_i|, \tag{3}$$

where S_d and S_u represent the reference downcast and upcast salinity profiles, respectively. In Eq. (2), i represents the profile number, and N is the total number of profiles (N = 495). AMSD is the absolute mean salinity difference averaged over all profiles at each isopycnal levels, forming an averaged profile. In Eq. (3), j represents the index of vertical sampling points (isopycnal levels), and M is the total number of sampling points. AMSD$_{\text{ver-avg}}$ is the vertical-averaged AMSD, calculated by averaging the AMSD profile vertically, yielding a single representative value.

(2) Error reduction rate (ERR)

The ERR quantifies the improvement in salinity difference between the reference downcast and upcast profiles after thermal lag correction, which is calculated by

$$\mathrm{ERR} = \frac{\mathrm{AMSD}_{\text{ver-avg,original}} - \mathrm{AMSD}_{\text{ver-avg,corrected}}}{\mathrm{AMSD}_{\text{ver-avg,original}}} \times 100\%, \tag{4}$$

where AMSD$_{\text{ver-avg,original}}$ denotes vertical-averaged AMSD for the original (uncorrected) profile, and AMSD$_{\text{ver-avg,corrected}}$ represents the corresponding profile after all corrections.

3 Thermal lag correction

3.1 *Principles of thermal lag correction*

Thermal lag correction is mainly based on Lueck's

theoretical model (Lueck, 1990), and can be achieved via two approaches: (1) estimating conductivity at the thermistor location (i.e., outside the conductivity cell) or (2) estimating temperature inside the conductivity cell.

For the first approach, the conductivity correction ($C_T(k)$) can be expressed as follows (Lueck and Picklo, 1990):

$$C_T(k) = -bC_T(k-1) + \gamma a[T(k) - T(k-1)], \quad (5)$$

where $C_T(k)$ is the thermal-lag correction to conductivity at the k-th sampling point within a profile, $T(k)$ is the measured temperature at that point, and γ is the sensitivity of conductivity to temperature. The coefficients a and b are given by

$$a = \frac{4f_N\alpha\beta}{1+4f_N\beta}, \quad (6)$$

$$b = 1 - \frac{2a}{\alpha}, \quad (7)$$

where f_N is the Nyquist sampling frequency, α and β are the correction parameters of error amplitude and time lag constant, respectively. Morison et al. (1994) showed that there is a relation between α, β and flow speed (flushing rate) through the conductivity cell:

$$\alpha = 0.013\,5 + \frac{0.024\,6}{V}, \quad (8)$$

$$\beta = 7.149\,9 + \frac{2.785\,8}{\sqrt{V}}, \quad (9)$$

where V is the flow speed (in m/s) through the conductivity cell. For pumped CTDs, the flow speed remains relatively steady, resulting in constant values for α and β. However, for unpumped CTDs, the parameters α and β shall not be calculated using Eqs (8) and (9) since the assumption of constant flow speed is no longer satisfied. To solve this problem, Garau et al. (2011) modified the expressions for α and β as follows:

$$\alpha(k) = \alpha_o + \frac{\alpha_s}{V_f(k)}, \quad (10)$$

$$\beta(k) = \beta_o + \frac{\beta_s}{\sqrt{V_f(k)}}, \quad (11)$$

where the subscripts o and s indicate the offsets and slopes for α and β, respectively. $V_f(k)$ is the speed of the flow, which is a variable parameter. To estimate α and β [Eqs (10) and (11)], it is essential to determine the parameters [α_o, α_s, β_o, β_s]. To sum up, the first thermal lag correction approach estimates the actual conductivity by adding the conductivity correction (C_T) to the measured conductivity (C_{meas}) (Garau et al., 2011), and then calculates salinity using the actual conductivity along with the measured temperature.

For the second approach, the temperature correction ($T_T(k)$) can be expressed as follows (Morison et al., 1994):

$$T_T(k) = -bT_T(k-1) + a[T(k) - T(k-1)], \quad (12)$$

where coefficients a and b are computed according to Eqs (6) and (7). This approach is simpler and computationally more efficient than the first approach, because it does not rely on the estimate of sensitivity γ. In this case, subtracting the temperature correction (T_T) from the measured temperature (T_{meas}) gives the actual temperature (Garau et al., 2011), which can be used to calculate salinity along with the measured conductivity.

3.2 *Practical thermal lag correction methods*

3.2.1 *Garau method*

Building upon established theoretical foundations, Garau et al. (2011) developed an innovative methodology for correcting thermal lag errors in unpumped CTD data from Slocum gliders. This method is not only flexible to apply to CTD profiles from autonomous platform, but can also incorporates the variations in glider speed. Subsequently, Troupin et al. (2015) extended this approach to pumped CTD systems. This thermal lag correction algorithm was made publicly accessible as a MATLAB toolbox, which has been widely adopted in numerous studies (e.g., Liu et al., 2015; Ruiz et al., 2012; Yang et al., 2022). The toolbox operates in two modes: (1) for pumped CTD, it returns a two-element parameter vector [α, β] representing error magnitude and error time constant, respectively; (2) for unpumped CTD, it returns a four-element vector [α_o, α_s, β_o, β_s] that includes both offset and slope parameters for error magnitude and error time constant. In our implementation, we utilize the pumped CTD code from this toolbox to derive the α and β parameters for each pair of downcast and upcast profiles. For convenience, we designate this approach as the Garau method. Figure 3a illustrates the selection scheme of reference profiles employed in the Garau method.

3.2.2 *Segmented method*

In the Garau method, thermal lag correction is implemented by selecting downcast and upcast profiles from a single glider dive as a reference pair (Fig. 3a, blue lines). However, due to the glider's sawtooth sampling trajectory, these reference profiles exhibit natural spatiotemporal discrepancies in shallow waters (e.g., above the pycnocline). To address this limitation and better satisfy the fundamental assumption of thermal lag correction, Wang et al. (2020) proposed an approach that used distinct selection strategies for reference profiles in different ocean layers. Building upon this foundation, we implement the seg-

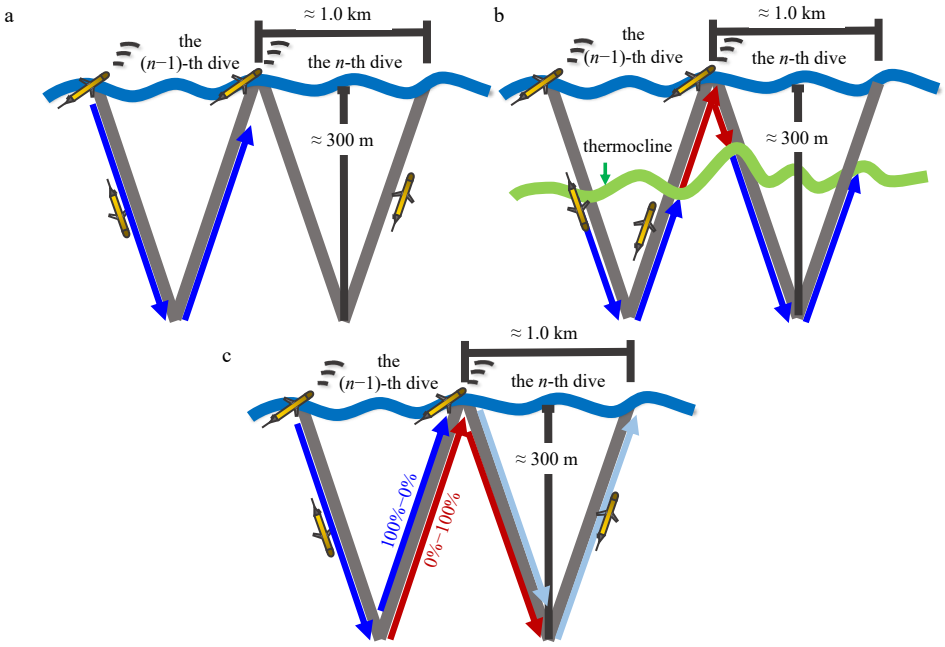


Fig. 3. Conceptual diagrams of glider trajectories and reference profiles for thermal lag correction using the Garau (a), segmented (b), and weighted (c) methods. The sawtooth pattern represents the glider sampling trajectory, with the ocean surface indicated by the blue curves. The horizontal distance between consecutive surface points is approximately 1 km. For simplicity, the underwater paths are illustrated as straight lines. a. In the Garau method, the downcast and upcast from a single dive cycle (blue lines) are paired as reference profiles. b. In the segmented method, the reference pair for the upper ocean (σ_θ < 24.34 kg/m^3) consists of the upcast from the (n − 1)-th dive and the downcast from the n-th dive (red lines). For the lower ocean (σ_θ > 24.34 kg/m^3), the reference pair is the downcast and upcast from the n-th dive (blue lines). The 24.34 kg/m^3 isopycnal surface (green line) separates these two layers. c. In the weighted method, the first reference dataset follows the Garau method (blue lines), while the second dataset follows the anti-Garau method (see Section 3.2.2; red lines). The percentages in blue and red illustrate the varying weights assigned to each dataset.

mented method adopting a similar dual-reference scheme: the upper ocean (σ_θ < 24.34 kg/m^3) correction employs data from the upcast of the (n − 1)-th glider dive and the downcast of the n-th glider dive as a pair of reference profiles (Fig. 3b, red lines), while the lower ocean (σ_θ > 24.34 kg/m^3) correction uses the downcast and upcast profiles from the n-th dive (Fig. 3b, blue lines). The transition depth between the upper and lower ocean is determined by analyzing the original (uncorrected) absolute mean salinity difference (AMSD$_{ori}$) curves from two complementary datasets. The determination procedure for segmentation points involves three steps.

(1) Compute the AMSD$_{ori}$ using reference profiles selected by the Garau method (i.e., downcast and upcast from a single dive; Fig. 3a, blue lines).

(2) Repeat the AMSD$_{ori}$ calculation using the anti-Garau method, where the reference profiles are taken from the upcast of the (n − 1)-th dive and the downcast of the n-th dive (Fig. 3c, red lines).

(3) Identify the isopycnal surface where the AMSD$_{ori}$ curves from the Garau and anti-Garau methods first intersect, located near the peak of the AMSD$_{ori}$ curves (Fig. S2). This surface is then selected as the segmentation point for the segmented method.

Notably, the anti-Garau method demonstrates slightly lower AMSD$_{ori}$ values in lighter water masses (σ_θ < 24.34 kg/m^3), while the Garau method yields smaller AMSD$_{ori}$ values in denser water masses (σ_θ > 24.34 kg/m^3; Fig. S2). Hence, we designate the isopycnal surface of 24.34 kg/m^3 as the division point for the segmented method. Specifically, for the upper ocean (σ_θ < 24.34 kg/m^3), salinity correction uses reference profiles from the upcast of the (n − 1)-th dive and the downcast of the n-th dive; for the lower ocean (σ_θ > 24.34 kg/m^3), we use reference profiles from the downcast and upcast of the n-th dive (Fig. 3b).

3.2.3 *Weighted method*

Building upon the segmentation concept, here we propose the weighted method to enhance the spatial and temporal consistency of each pair of reference profiles. This approach consists of four steps.

(1) Perform thermal lag correction using reference profiles from a single dive (Fig. 3c, blue lines) following the Garau method, generating the first corrected salinity dataset.

(2) Apply thermal lag correction using reference profiles from consecutive dives (i.e., upcast from the (n − 1)-th dive and the downcast from the n-th dive; Fig. 3c, red lines) following the anti-Garau method, yielding the sec-

ond corrected salinity dataset. This dual-correction strategy ensures that each profile (except for the initial and final dives) has two independent salinity datasets.

(3) Interpolate the above two datasets onto a weighting transition zone with a potential density interval of 0.002 kg/m^3. This zone is defined to encompass the glider's maximum dive depth. For the 300K001 glider, which has a maximum dive depth of approximately 300 m, the weighting transition zone corresponds to the isopycnal range of 22−26 kg/m^3. This range should be adjusted accordingly if the glider's maximum dive depth or the ambient potential density changes.

(4) Combine the two interpolated datasets using a linear weighting scheme based on the vertical isopycnal positions. Specifically, within the 22−26 kg/m^3 weighting transition zone (at the interval of 0.002 kg/m^3), each isopycnal surface is assigned a specific weight for the Garau and anti-Garau methods. The final salinity value is computed as the weighted average of the salinity values from the two methods. For example, on the top isopycnal surface (σ_θ = 22 kg/m^3), the anti-Garau method is assigned 100% weight while the Garau method is 0%; on the second top surface (σ_θ = 22.002 kg/m^3), weights shift to 99.95% (anti-Garau method) and 0.05% (Garau method), and so on.

This proposed weighted method ensures that salinity values derived from the Garau method dominate at greater depths, while those from the anti-Garau method dominate near the sea surface. By integrating the two approaches through weighted averaging, we leverage their respective strengths while minimizing their individual limitations.

4 Results

4.1 *Comparing the weighted method with existing methods*

To evaluate the performance of the weighted method, we conduct a systematic comparison between its corrected salinity data and those by existing methods (Garau and segmented methods). The assessment starts from a pair of profiles followed by a statistical comparison across all profiles.

4.1.1 *A pair of salinity profiles*

We select a typical pair of glider-measured salinity profiles to conduct the comparison. Influenced by the thermal lag effect, the original downcast and upcast exhibit significant salinity differences, with the salinity measured in the downcast profile consistently higher than the upcast in both pressure (Figs 4a−c) and isopycnal coordinates (Figs 4g−i). After correction, all three methods (the Garau, segmented, and weighted methods) substantially reduced these salinity differences between the reference profiles (only above σ_θ = 24.3 kg/m^3 isopycnal surface is shown for a better view; Figs 4d−f and j−l), demonstrating that thermal lag errors can be effectively mitigated by both the proposed weighted method and existing methods (Garau and segmented methods). Notably, while vertical mismatches persist between downcast and upcast of the corrected profiles in pressure coordinates (Figs 4d−f), these mismatches are significantly alleviated in isopycnal coordinates (Figs 4j−l). This might be due to the passage of internal waves during the measurement period that induced vertical displacements of isopycnal surfaces. Hence the misalignments seen in pressure coordinates would largely disappear in isopycnal coordinates. This finding underscores the importance of performing and evaluating thermal lag correction in isopycnal coordinates or *T*-*S* diagrams, particularly for salinity measurements influenced by internal waves.

The initial evaluation using a pair of profiles indicated that the weighted method reduces thermal lag errors as effectively as existing methods (Garau and segmented methods). To further validate the performance of the weighted method, we conducted a comprehensive statistical analysis using 495 profile pairs.

4.1.2 *Statistical analyses across all salinity profiles*

By calculating the salinity difference (SD) between the downcast and upcast of each pair of the 495 profiles, it is shown that the original SD values span a range of ±0.15 (Figs 5a−c), while the corrected SD show substantially narrower ranges, depending on the methods used for correction (Figs 5d−f). Notably, positive SD values were substantially reduced, whereas negative SD values showed minimal change, as expected from the thermal lag effects. Assuming that seawater temperature decreases with depth (which is often the case), thermal lag effect would induce a slight positive salinity error during the downcast profiling and a slight negative salinity error during the upcast profiling. Excluding errors induced by other processes, the downcast-minus-upcast SD caused by thermal lag effect should be positive (Chu et al., 2020). The marked reduction in positive SD values confirms the effectiveness of all three methods in mitigating thermal lag errors. Among them, the weighted method yields the narrowest SD range (±0.05; Fig. 5f) for corrected profiles, along with the smallest vertical-averaged AMSD (0.003 0) and highest ERR (90.3%) compared to the existing methods (Garau and segmented methods; Table 1). These results support our hypothesis that the effectiveness of thermal lag correction improves when reference profiles are more closely matched in time and space, and thus better satisfies the assumptions of the thermal lag correction.

Compared with the segmented method, the weighted method eliminates artificial salinity spikes (Figs 5e and f). The segmented method corrects salinity using different reference profiles above and below a predefined division point, potentially introducing discontinuous and artificial salinity spikes. In contrast, the weighted method operates without preset division points, thereby naturally removes such discontinuities. Besides, the larger AMSD in the segmented method compared with the Garau method

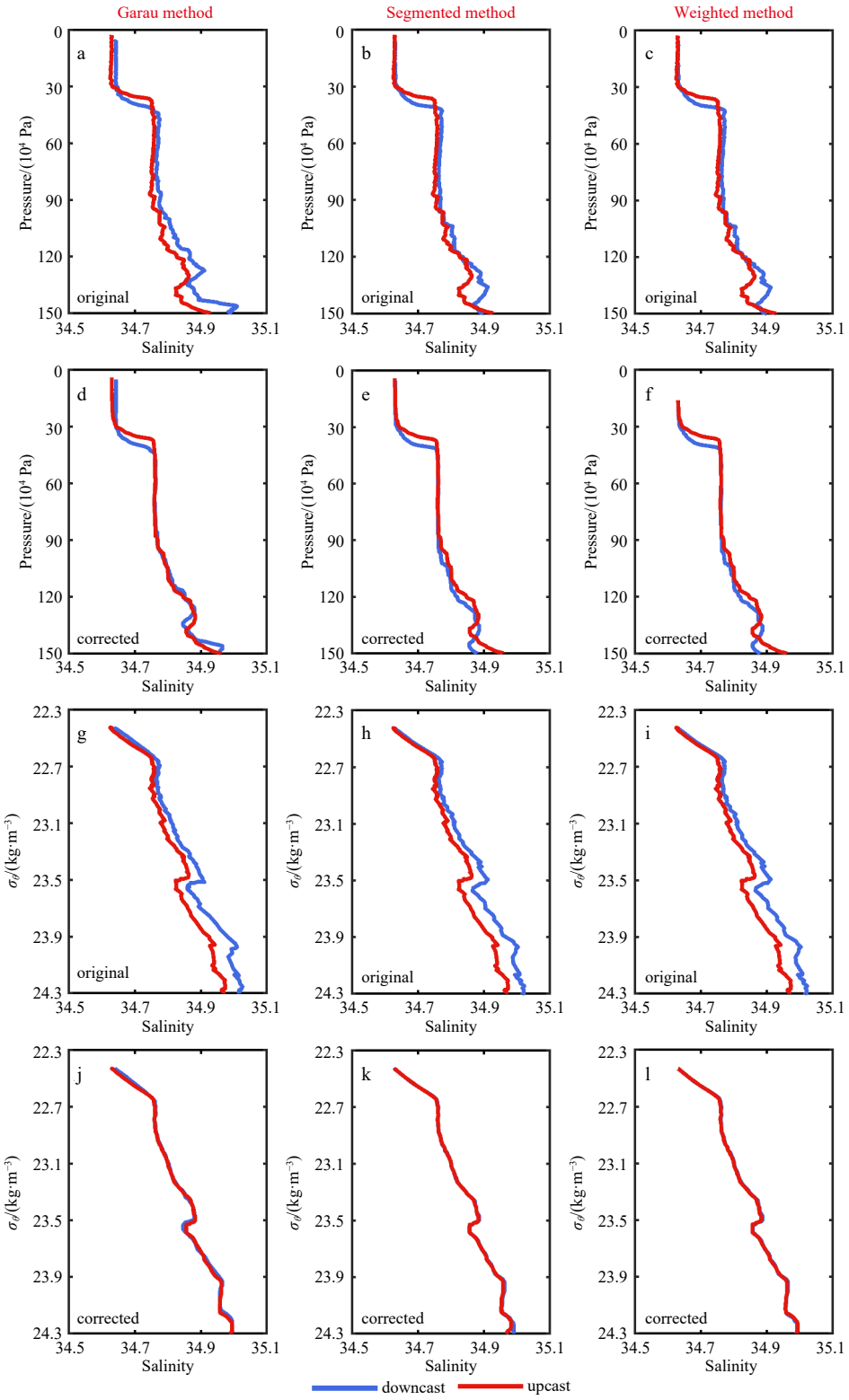


Fig. 4. Comparisons of the weighted method with existing methods (Garau and segmented methods) in both pressure and isopycnal coordinates. a–f. Salinity profiles in pressure coordinates, and g–l. corresponding profiles in isopycnal coordinates. a–c and g–i show original (uncorrected) salinity profiles, while d–f and j–l display the corrected profiles. Blue lines and red lines indicate downcast and upcast salinity profiles, respectively.

(Table 1) is caused by systematic errors at the division points. This is supported by the fact that when data near division points are excluded, the segmented method's AMSD becomes smaller than the Garau method's (Table 1, values in parentheses).

These findings demonstrate that the weighted method outperforms existing methods (Garau and segmented methods) in thermal lag correction. Specifically, it offers

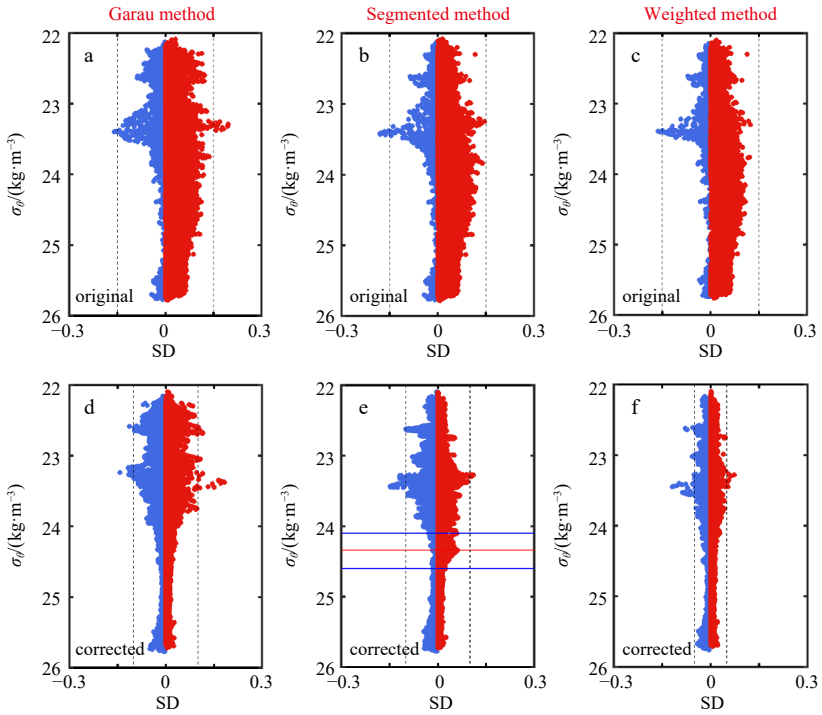


Fig. 5. Distribution of salinity differences (SD) between reference profiles for the Garau (a, d), segmented (b, e), and weighted (c, f) methods in isopycnal coordinates. a–c Original (uncorrected) SD distributions with dashed lines indicate the ±0.15 range. d–f Corrected SD distributions, dashed lines mark ±0.10 in d and e and ±0.05 in f. In e, red line denotes the 24.34 kg/m^3 isopycnal surface (division point), while blue lines indicate the σ_θ = 24.1 kg/m^3 and σ_θ = 24.6 kg/m^3 isopycnal surfaces (corresponding to transition zone near the division point; see Table 1), respectively.

Table 1. Vertical-averaged absolute mean salinity differences ($AMSD_{ver\text{-}avg}$) between the referenced downcast and upcast of each pair of the 495 profiles

Method	Original $AMSD_{ver\text{-}avg}$	Corrected $AMSD_{ver\text{-}avg}$	Error reduction rate (ERR)/%
Garau method	0.031 2	0.004 7	84.9
Segmented method	0.030 9	0.004 9	84.1
	(0.028 5)	(0.003 5)	(87.7)
Weighted method	0.030 9	0.003 0	90.3

Note: Parenthetical values indicate the $AMSD_{ver\text{-}avg}$ and ERR calculated after excluding data within the transition zone (between σ_θ = 24.1 kg/m^3 and σ_θ = 24.6 kg/m^3 isopycnal surfaces) for the segmented method.

two key advantages: (1) It achieves the smallest corrected $AMSD_{ver\text{-}avg}$ (0.003 0) and highest ERR (90.3%) among the tested methods; (2) It avoids introducing the artificial salinity spikes inherent to the segmented method at the division points, thereby maintaining smoothness for the corrected profile.

4.2 *Validation of the weighted method against SBE 911plus CTD data*

To validate the accuracy of salinity profiles corrected by the weighted method, we select five synchronous SBE 911plus CTD (for simplicity, denoted as CTD) casts matching glider profiles for comparison. These CTD casts satisfy the following criteria: (1) temporal difference < 2 h (Table S1), and (2) spatial separation < 0.1° (about 10 km) in both longitude and latitude (Fig. 1, green circles for glider positions and yellow rectangles for CTD stations).

The comparison demonstrates close agreement between salinity profiles corrected using the weighted method and shipboard CTD measurements throughout the water column (Figs 6a–e). Notably, the weighted method accurately captures salinity variations even in the thermocline region where temperature gradients are the largest. Statistical analysis reveals a strong linear correlation (about 1.0) between weighted method-corrected glider salinity and CTD measurements (Fig. 6f). While minor discrepancies appear in the upper-ocean water column (σ_θ < 24 kg/m^3) for Profile G4-2—potentially attributable to other physical processes—the overall consistency between the two datasets (glider-based salinity measurements vs. CTD salinity data) provides robust effectiveness of the weighted method in thermal lag correction.

5 Discussion

5.1 *Impact of fronts on profile corrections*

Theoretically, if all profiles satisfy the basic assumption of the thermal lag correction—the upcast and downcast sampling the same water mass—the corrected profiles should converge perfectly. However, some corrected salinity profiles still exhibit notable misalignments between the downcast and upcast (e.g., Fig. 7a). We suspect

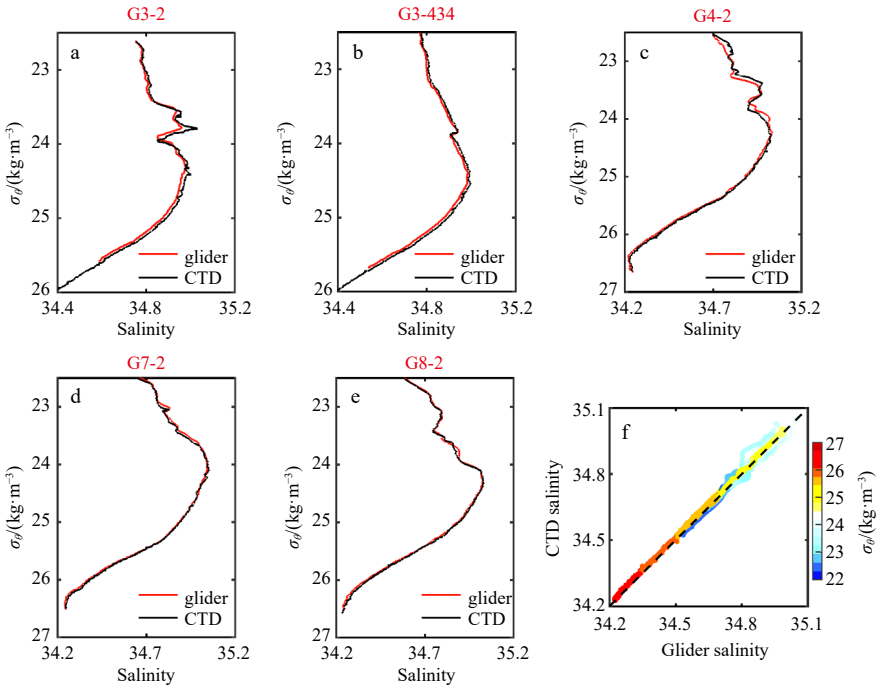


Fig. 6. Validation of the weighted method against SBE 911plus CTD data in isopycnal coordinates. a–e. Comparison of salinity profiles: red lines show glider-measured salinity profiles corrected by the weighted method, and black lines display SBE 911plus CTD measurements. The sampling locations of the glider and SBE 911plus CTD profiles are indicated by green circles and yellow rectangles, respectively, in Fig. 1. Profile identifiers are shown in the panel titles. For example, "G3-2" denotes the mean profile obtained by averaging the downcast and upcast profiles of the second profile pair collected by Glider 3. Note that the vertical scales differ across a–e to accommodate the varying maximum dive depths: approximately 300 m for G3-2 and G3-434, and approximately 500 m for G4-2, G7-2, and G8-2. f. Scatterplot demonstrating the correlation between the salinity profiles from the two sources.

this is because the glider was traversing frontal areas where strong lateral thermohaline gradients exist along isopycnals; in this case the glider downcast and upcast were profiling different water masses, and thus violate the above assumption.

To verify this hypothesis, we examine a pair of adjacent salinity profiles (upcast from the $(n-1)$-th dive and downcast from the n-th dive) collected near the edge of a cyclonic eddy on April 12, 2019 (Fig. 7e, magenta point). These profiles are selected as reference pairs (denoted as m) given their high consistency (weight) in the shallow water. Our analysis reveals persistent misalignments after corrections, most pronounced along the σ_θ = 22.8 kg/m^3 and σ_θ = 23.7 kg/m^3 isopycnals (Fig. 7a). Intriguingly, the upcast profile of Pair m shows better alignment with the preceding profile ($m-1$) (Fig. 7b), while its downcast profile aligns more closely with the subsequent profile ($m+1$) (Fig. 7c). This pattern is quantitatively supported by absolute salinity difference distribution (Fig. 7d) and vertical-averaged absolute salinity difference ($ASD_{ver\text{-}avg}$) values: the $ASD_{ver\text{-}avg}$ value between the downcast and upcast of Pair m (0.008 5) exceeds that either between its upcast and the preceding profile (0.006 5) or between its downcast and the subsequent profile (0.004 0). These results suggest that the downcast and upcast of Pair m indeed sampled distinct water masses. As the upcast and downcast profiles of Pair m are located near the edge of an eddy (Fig. 7e, magenta point), where relatively strong density gradients (i.e., fronts) are expected (e.g., Capet et al., 2008). Hence these glider measurements serve as partial observational evidence for the presence of fronts at eddy peripheries, as well as their impact on the observed salinity misalignments.

To further examine the relationship between salinity misalignments and frontal structures, we analyze the cross-sectional distributions of potential temperature (Fig. 8a), salinity (Fig. 8b), and salinity gradients (Fig. 8c) along the trajectory of glider 300K001 from March 29 to April 14, 2019 in isopycnal coordinates, all derived from profiles corrected by the weighted method. The salinity gradients (Fig. 8c) and $ASD_{ver\text{-}avg}$ (Fig. 8d) serve as indicators of frontal positions. Our analysis reveals that regions with strong temperature and salinity variability in isopycnal coordinates (Figs 8a–b) correspond precisely with areas of enhanced salinity gradients and large $ASD_{ver\text{-}avg}$ values (Figs 8c–d). This demonstrates that when glider traverses frontal zones, its downcast and upcast profiles sample distinct water masses, resulting in significant salinity differences, particularly in regions with pronounced thermohaline gradients.

Further investigation shows that regions with large salinity gradients and elevated $ASD_{ver\text{-}avg}$ values are gen-

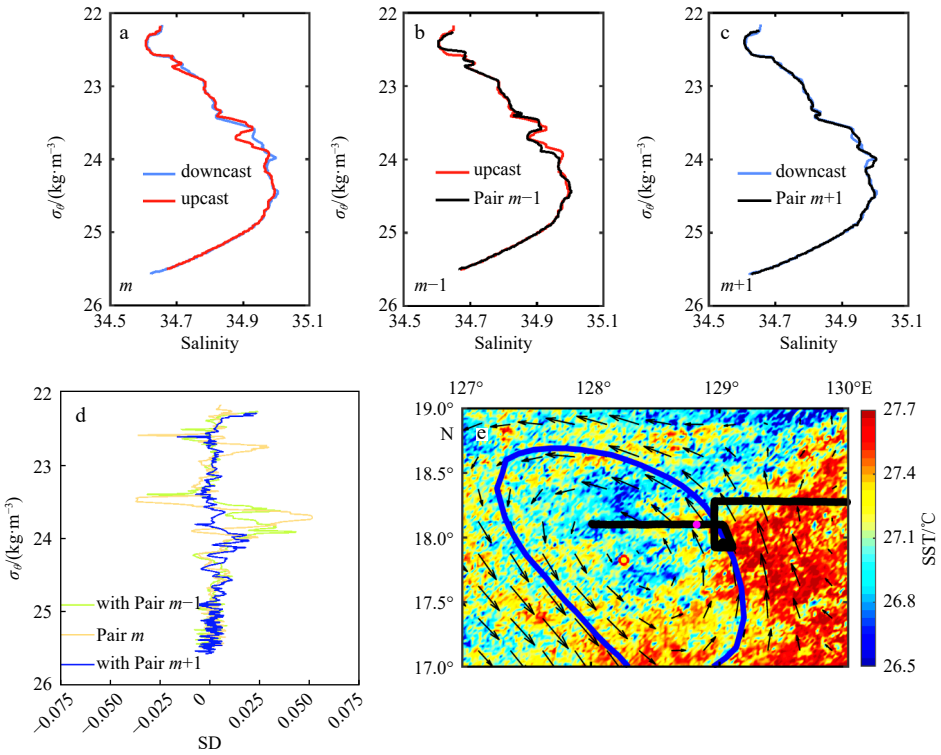


Fig. 7. Salinity profiles near a cyclonic eddy periphery in isopycnal coordinates. a. Salinity profiles from Pair *m* showing downcast (blue) and upcast (red) measurements. b. Comparison between Pair *m* upcast (red) and its preceding profile (black). c. Comparison between Pair *m* downcast (blue) and its subsequent profile (black). d. Salinity differences (SD) between Pair *m* downcast and upcast (orange), Pair *m* upcast, and its preceding profile (light green), and Pair *m* downcast and its subsequent profile (blue). e. Daily sea surface temperature (SST) from Himawari-8 (color shading) overlaid with surface geostrophic currents (black arrows) on April 12, 2019. The blue curve and the red circle mark the edge and center of the observed eddy. The black line traces the trajectory of glider 300K001. The magenta point marks the sampling position of glider profile Pair *m*.

erally associated with abnormal values of the thermal lag correction parameters (α and β), albeit with some exceptions (Figs 8c–e). These correlations suggest that frontal structures and the associated thermohaline anomalies introduce uncertainties into thermal lag correction, and thus underscore the profound impact of mesoscale and submesoscale features on the accuracy of glider-based salinity measurements (e.g., Qiu et al., 2025).

5.2 *Limitations of the weighted method*

While the proposed weighted method demonstrates improved performance over existing approaches, several limitations are worthy of discussion. First, the linear weighting scheme relies on the vertical position of isopycnals while neglecting the influence of vertical physical processes (e.g., thermocline variabilities) on thermal lag correction. Future work could further optimize the weighting configuration by incorporating specific physical processes. Second, the validation of salinity corrections in frontal regions (e.g., eddy peripheries) remains challenging given the lack of synchronized SBE 911plus CTD measurements. Future studies should acquire concurrent high-resolution CTD data in frontal zones to enable a more robust validation of the weighted method.

6 Conclusions

This study presents a modified thermal lag correction approach, termed the weighted method, specifically designed for glider-based salinity measurements. This approach leverages the distinctive V-shaped sampling pattern of gliders through a linear weighting scheme taking into account the spatiotemporal proximity of reference profiles. Our key findings demonstrate:

(1) When compared with existing methods (Garau and segmented methods), the weighted method shows superior performance in thermal lag correction, achieving both a lower vertical-averaged absolute mean salinity difference (0.003 0) between the corrected downcast and upcast profiles and a higher error reduction rate (90.3%). The weighted method also eliminates artificial salinity spikes that are characteristic of the segmented method.

(2) The weighted method operates thermal lag correction in isopycnal coordinates, which naturally removes distortions caused by internal wave-induced isopycnal displacements, and thus possesses an inherent advantage over those based on pressure coordinates.

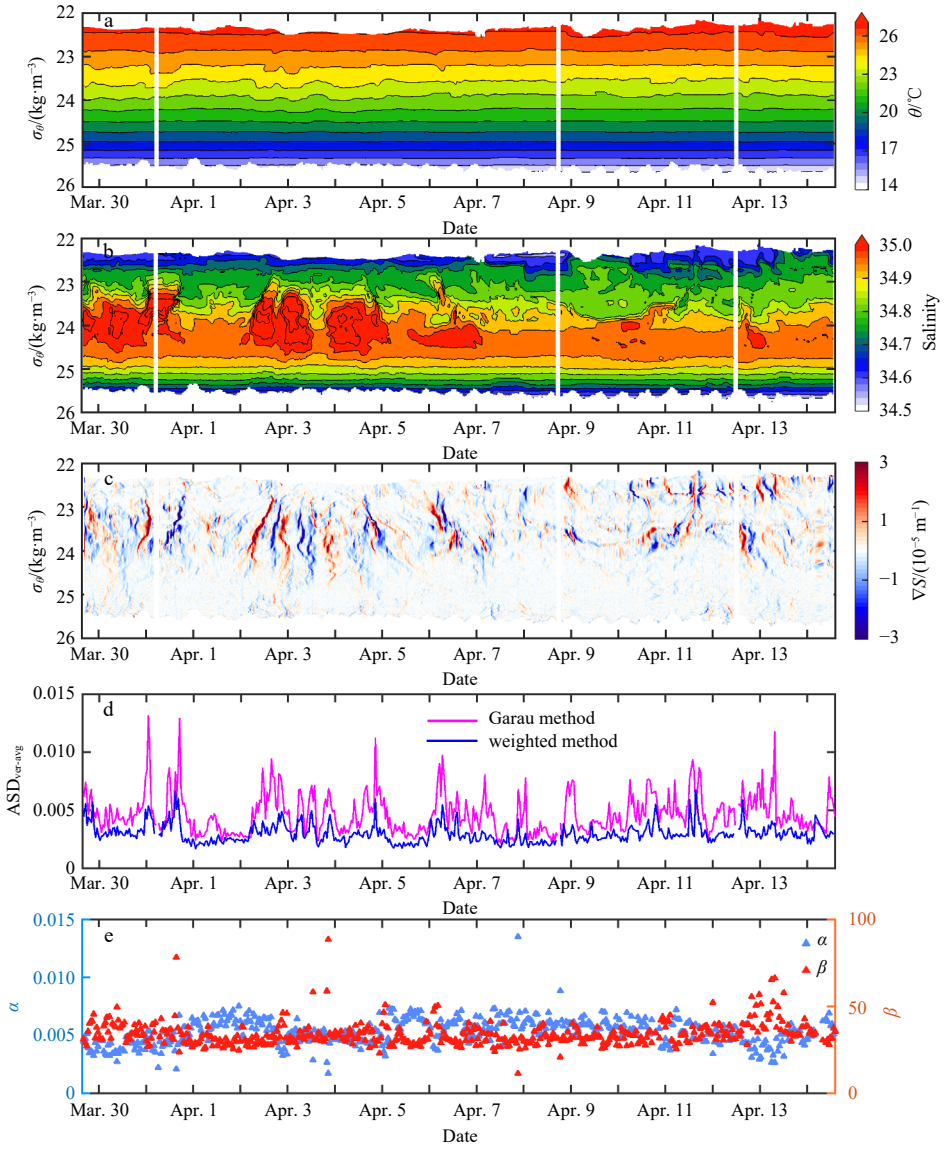


Fig. 8. Cross-sectional distributions along the trajectory of glider 300K001 of potential temperature (θ) (a), salinity (b), and salinity gradients (∇S, 10^{-5} m^{-1}) (c) after correction by the weighted method, the vertical-averaged absolute salinity difference ($ASD_{ver\text{-}avg}$) both for Garau (magenta line) and weighted methods (blue line) (d), and thermal lag correction parameters α (blue triangles) and β (red triangles) from Garau method (e). The sampling period was from March 29, 2019 at 15:28:00 to April 14, 2019 at 14:18:30 (Beijing time, UTC+8).

(3) Validation against the SBE 911plus CTD measurements confirms the reliability of the weighted method in obtaining accurate glider-measured salinity data after thermal lag correction.

(4) In regions with strong salinity gradients (e.g., fronts, eddy boundaries), mismatches between the corrected downcast and upcast profiles can still exist because the glider downcast and upcast would be sampling different water masses in such regions, which violates the basic assumption of thermal lag correction.

Acknowledgements

We thank Cao Zhiyong and the crews of R/V *Tan Kah Kee* for acquiring the numerous observation data used in this study. We are also grateful to members of the dynamical oceanography group (DyOG) of Xiamen University for helpful discussions.

References

Bishop C M. 2008. Sensor dynamics of of autonomous underwater gliders [dissertation]. Newfoundland: Memorial University of Newfoundland

Capet X, Campos E J, Paiva A M. 2008. Submesoscale activity over the Argentinian shelf. Geophysical Research Letters, 35(15): L15605, doi: 10.1029/2008gl034736

Chu Fushuo, Si Zongshang, Pang Chongguang, et al. 2020. Thermal lag correction from a glider payload CTD for poor temperature data. Pure and Applied Geophysics,

177(6): 3039–3051, doi: 10.1007/s00024-019-02359-1

Fofonoff N P, Millard Jr R C. 1983. Algorithms for computation of fundamental properties of seawater: UNESCO technical papers in marine science 44. Paris: UNESCO, 1–53

Garau B, Ruiz S, Zhang W G, et al. 2011. Thermal lag correction on Slocum CTD glider data. Journal of Atmospheric and Oceanic Technology, 28(9): 1065–1071, doi: 10.1175/jtech-d-10-05030.1

Hu Zhendong, Lin Hongyang, Liu Zhiyu, et al. 2023. Observations of a filamentous intrusion and vigorous submesoscale turbulence within a cyclonic mesoscale eddy. Journal of Physical Oceanography, 53(6): 1615–1627, doi: 10.1175/jpo-d-22-0189.1

Johnson G C, Toole J M, Larson N G. 2007. Sensor corrections for Sea-Bird SBE-41CP and SBE-41 CTDs. Journal of Atmospheric and Oceanic Technology, 24(6): 1117–1130, doi: 10.1175/jtech2016.1

Liu Yonggang, Weisberg R H, Lembke C. 2015. Glider salinity correction for unpumped CTD sensors across a sharp thermocline. In: Liu Yonggang, Kerkering H, Weisberg R H, eds. Coastal Ocean Observing Systems. San Diego: Academic Press, 305–325, doi: 10.1016/b978-0-12-802022-7.00017-1

Lueck R G. 1990. Thermal inertia of conductivity cells: theory. Journal of Atmospheric and Oceanic Technology, 7(5): 741–755, doi: 10.1175/1520-0426(1990)007<0741:TIOCCT>2.0.CO;2

Lueck R G, Picklo J J. 1990. Thermal inertia of conductivity cells: observations with a Sea-Bird cell. Journal of Atmospheric and Oceanic Technology, 7(5): 756–768, doi: 10.1175/1520-0426(1990)007<0756:TIOCCO>2.0.CO;2

Mason E, Pascual A, McWilliams J C. 2014. A new sea surface height-based code for oceanic mesoscale eddy tracking. Journal of Atmospheric and Oceanic Technology, 31(5): 1181–1188, doi: 10.1175/jtech-d-14-00019.1

Morison J, Andersen R, Larson N, et al. 1994. The correction for thermal-lag effects in Sea-Bird CTD data. Journal of Atmospheric and Oceanic Technology, 11(4): 1151–1164, doi: 10.1175/1520-0426(1994)011<1151:TCFTLE>2.0.CO;2

Pegliasco C, Delepoulle A, Mason E, et al. 2022. META3.1exp: A new global mesoscale eddy trajectory atlas derived from altimetry. Earth System Science Data, 14(3): 1087–1107, doi: 10.5194/essd-14-1087-2022

Qiu Chunhua, Du Zhenyang, Tang Haibo, et al. 2025. A high-resolution temperature–salinity dataset observed by autonomous underwater vehicles for the evolution of mesoscale eddies and associated submesoscale processes in the South China Sea. Earth System Science Data, 17(7): 3189–3202, doi: 10.5194/essd-17-3189-2025

Rudnick D L. 2016. Ocean research enabled by underwater gliders. Annual Review of Marine Science, 8(1): 519–541, doi: 10.1146/annurev-marine-122414-033913

Rudnick D L, Davis R E, Eriksen C C, et al. 2004. Underwater gliders for ocean research. Marine Technology Society Journal, 38(2): 73–84, doi: 10.4031/002533204787522703

Ruiz S, Renault L, Garau B, et al. 2012. Underwater glider observations and modeling of an abrupt mixing event in the Upper ocean. Geophysical Research Letters, 39(1): L01603, doi: 10.1029/2011GL050078

Stommel H. 1989. The Slocum mission. Oceanography, 2(1): 22–25, doi: 10.5670/oceanog.1989.26

Troupin C, Beltran J P, Heslop E, et al. 2015. A toolbox for glider data processing and management. Methods in Oceanography, 13–14: 13–23, doi: 10.1016/j.mio.2016.01.001

Wang Yanhui, Luo Chenyi, Yang Shaoqiong, et al. 2020. Modified thermal lag correction of CTD data from underwater gliders. Journal of Coastal Research, 99(sp1): 137–143, doi: 10.2112/SI99-020.1

Yang Dehou, Jing Chunsheng, Huang Jiang. 2022. Discussion on the correction method of thermal lag effect deviation in salinity data of sea-wing glider. Journal of Applied Oceanography (in Chinese), 41(1): 156–165, doi: 10.3969/J.ISSN.2095-4972.2022.01.019

Supplementary information:

Fig. S1. Pressure variations with sampling points for four abnormal profiles. The maximum sampling depth of the first profile is approximately 120 m, which is significantly shallower than the glider's preset depth. Profiles 52 and 328 are pressure-anomalous profiles. Profile 444 contains only upcast data.

Fig. S2. Comparison of original (uncorrected) absolute mean salinity difference ($AMSD_{ori}$) between the Garau and anti-Garau methods in isopycnal coordinates. a. $AMSD_{ori}$ profiles for the Garau method (blue line) and anti-Garau method (red line). b. Magnified view of the red boxed area in a. The black dashed line in both panels indicates the σ_θ = 24.34 kg/m^3 isopycnal surface. The grey dashed lines in b denote the σ_θ = 24.462 kg/m^3 and σ_θ = 24.48 kg/m^3 isopycnal surfaces.

Table S1. Sampling time and position records for glider and SBE 911plus CTD measurements

The supplementary information is available online at https://doi.org/10.1007/s13131-026-2700-8 and http://www.aosocean.com/. The supplementary information is published as submitted, without typesetting or editing. The responsibility for scientific accuracy and content remains entirely with the authors.